Bimodal and Gaussian Ising spin glasses in dimension two

P. H. Lundow[1] and I. A. Campbell[2]

[1]*Department of Mathematics and Mathematical Statistics, Umeå University, SE-901 87, Sweden*

[2]*Laboratoire Charles Coulomb (L2C), UMR 5221 CNRS-Université de Montpellier, Montpellier, France*

(Received 28 June 2015; revised manuscript received 29 November 2015; published 11 February 2016)

An analysis is given of numerical simulation data to size $L = 128$ on the archetype square lattice Ising spin glasses (ISGs) with bimodal ($\pm J$) and Gaussian interaction distributions. It is well established that the ordering temperature of both models is zero. The Gaussian model has a nondegenerate ground state and thus a critical exponent $\eta \equiv 0$, and a continuous distribution of energy levels. For the bimodal model, above a size-dependent crossover temperature $T^*(L)$ there is a regime of effectively continuous energy levels; below $T^*(L)$ there is a distinct regime dominated by the highly degenerate ground state plus an energy gap to the excited states. $T^*(L)$ tends to zero at very large L, leaving only the effectively continuous regime in the thermodynamic limit. The simulation data on both models are analyzed with the conventional scaling variable $t = T$ and with a scaling variable $\tau_b = T^2/(1 + T^2)$ suitable for zero-temperature transition ISGs, together with appropriate scaling expressions. The data for the temperature dependence of the reduced susceptibility $\chi(\tau_b, L)$ and second moment correlation length $\xi(\tau_b, L)$ in the thermodynamic limit regime are extrapolated to the $\tau_b = 0$ critical limit. The Gaussian critical exponent estimates from the simulations, $\eta = 0$ and $\nu = 3.55(5)$, are in full agreement with the well-established values in the literature. The bimodal critical exponents, estimated from the thermodynamic limit regime analyses using the same extrapolation protocols as for the Gaussian model, are $\eta = 0.20(2)$ and $\nu = 4.8(3)$, distinctly different from the Gaussian critical exponents.

DOI: 10.1103/PhysRevE.93.022119

I. INTRODUCTION

The canonical Edwards-Anderson (EA) model Ising spin glasses (ISGs) in dimension $d = 2$ have been the subject of very many numerical studies. There is now consensus supported by analytic arguments that the two archetype models, the ISGs on square lattices with near-neighbor interactions having distributions which are either Gaussian or bimodal ($\pm J$), have zero-temperature transitions [1,2]. For the Gaussian model, where the interaction distribution is continuous and the ground state is unique, there is now also general consensus concerning the low-temperature thermodynamic limit (ThL) behavior and exponents. In the bimodal case there is an "effectively continuous energy level distribution" regime coming down from high temperatures and ending with a crossover at a size-dependent temperature $T^*(L)$ to a ground-state-dominated regime [3]. Interpretations differ considerably concerning the critical exponents for the bimodal interaction model. We will give an analysis of accurate numerical Monte Carlo data in the ThL for bimodal and Gaussian model samples up to size $L = 128$. We use the temperature T or the inverse temperature β as convenient.

We first discuss the specific heat using data from the simulations together with independent data down to low temperatures and large sizes from Refs. [4] and [5]. Then we analyze the simulation data for other observables with the aim of obtaining reliable estimates for the critical exponents of the ThL regime, using both the conventional scaling variable T and a novel scaling variable compatible with the generic scaling approach for ISGs introduced in [6], adapted to a situation where $T_c = 0$. We find that the Gaussian model and the bimodal model in the ThL are not in the same universality class.

The two-dimensional (2D) Gaussian model is relatively clear-cut. Because $T_c = 0$ and the interaction distribution is continuous, there is a unique ground state (for each sample) and the low-temperature excitation distribution has no gap. The fact that the ground state is unique necessarily implies that for all L, as $T \to 0, \xi(T, L) \to \infty$ and the reduced susceptibility $\chi(T, L) \to L^2$. With T chosen as the critical scaling variable, the standard thermodynamic limit low-temperature critical expressions are $\xi(T) \sim T^{-\nu}$ and $\chi(T) \sim T^{-\gamma} = T^{-2\nu}$ because the critical exponent η is strictly zero. The critical behavior of both observables at low temperature is governed by the single exponent ν, which is related to the stiffness exponent through $\theta = -1/\nu$. Accurate zero-temperature domain wall stiffness measurements to large sizes [1,7–12] show that $\theta = -0.282(2)$, i.e., $\nu = 3.55(3)$.

In the 2D bimodal case the situation is complicated by two factors. First, the ground state is not unique but is massively degenerate; the zero-temperature entropy per spin is $S_0 = 0.078(5)k_B$ [12–14]. Second, the distribution of excited-state energy levels is not continuous but increases by steps of $4J$; in particular, there is an energy gap $4J$ between the ground state and the first excited state. One can write [4] the "naive" leading low-temperature finite-size limited specific heat expression

$$C_v(\beta, L) = \frac{16J^2 \exp[S_1(L) - S_0(L)] \exp(-4J/T)}{L^2 T^2}, \quad (1)$$

where $S_1(L), S_0(L)$ are the sample-averaged entropies of the first excited state and the ground state. Setting $J = 1$, a crossover temperature can then be defined by [5,15,16]

$$T^*(L) = 4/[S_1(L) - S_0(L)], \quad (2)$$

which separates the critical behavior in the low-temperature ground-state-dominated regime [with $C_v(\beta, L) \sim \exp(-4/T)/T^2$] and a $T > T^*(L)$ regime where the whole ensemble of higher energy states dominates the thermodynamics [3]. An explicit phenomenological expression for $T^*(L)$ derived from Eq. (5) of Ref. [16], which is consistent with the

raw data points [4,16] for $S_1(L) - S_0(L)$, is

$$\frac{4}{\exp\left(0.199 \ln\left\{\frac{\ln(6.28L^2)}{2} + L^2[\ln(L^2) - 1]\right\} + 0.473\right)}. \quad (3)$$

A much simpler droplet-based expression from [5] is $T^*(L) \approx L^{-1/2}$. $T^*(L)$ decreases with increasing L because the degeneracy of the excited states increases faster with L than that of the ground state. We will assume [3] that in the $T > T^*(L)$ ThL regime the data can be analyzed in the same way as if the energy level distribution were continuous. With this assumption the $T > T^*(L)$ regime will have "effectively continuous" energy level distribution of critical exponents with an effective ordering temperature T_c still zero. The ground-state-dominated regime at $T < T^*(L)$ is a finite-size effect which disappears in the infinite L limit.

A droplet analysis of ground-state measurements on large-sized samples [17] shows that $\eta \approx 0.22$, broadly consistent with a number of finite temperature simulation estimates [18–20]. However, it has been claimed that in the $T > T^*(L)$ regime the bimodal ISG can be considered to be effectively in the same universality class as the Gaussian ISG [3], meaning that the effective exponents are again $\eta = 0$ and $\nu = 3.55(5)$. In view of the basic definition of η in terms of the short-range limit of the spin-spin correlation function $G(r,T) = G\{r^{-\eta} \exp[r/\xi(T)]\}$, this claim is rather surprising.

A major difficulty in establishing the limiting $[T > T^*(L), L \to \infty, T \to 0]$ behavior for ISGs in dimension 2 [15] consists in finding an appropriate and reliable extrapolation procedure from simulation data necessarily restricted in size and in temperature because of the need to achieve good thermal equilibration at large sizes. This is a problem that we will address.

II. SIMULATIONS

The simulations were performed using the Houdayer cluster method [19] in combination with the exchange Monte Carlo [21] method. In the cluster step we first pick a random site i and compute its overlap $q_i = S_i^A S_i^B$, where S_i^A and S_i^B denote the spin for two different replicas. We then build an equal-q cluster along the nearest-neighbor interactions and flip all cluster spins in both replicas. We used four replicas which turned out to be remarkably efficacious. On each iteration the replicas are paired at random, and then, for each pair, a cluster update is performed, and the usual heat-bath spin update and exchange.

For all systems we used $\beta_{\max} = 3.0$. The number of temperatures were more than 250 for the smallest systems starting at $\beta_{\min} = 0.2$. With increasing system size the number of temperatures was decreased and $\beta_{\min}$ increased. For the largest system (bimodal J_{ij} with $L = 128$) 70 temperatures were used with $\beta_{\min} = 1.2$. The exchange rate was always at least 0.3 for all systems and temperatures. The systems were deemed equilibrated when the average $\langle q^2 \rangle$ for the systems at $\beta_{\max}$ appeared stable between runs. The number of equilibration steps increased with system size, for the bimodal $L = 128$ this took about 600 000 steps. After equilibration, at least 200 000 measurements were made for each sample for all sizes, taking place after every cluster-sweep-exchange step.

The usual observables were registered, the energy $E(\beta,L)$, the correlation length $\xi(\beta,L)$, the spin overlap moments $\langle|q|\rangle, \langle q^2\rangle, \langle|q|^3\rangle, \langle q^4\rangle$. Correlations $\langle E(\beta,L), U(\beta,L)\rangle$ between the energy and some observables $U(\beta,L)$ were also registered. Thermodynamic derivatives could then be evaluated through the usual $\partial U(\beta,L)/\partial\beta = \langle U(\beta,L), E(\beta,L)\rangle - \langle U(\beta,L)\rangle\langle E(\beta,L)\rangle$. Error estimates of observables and derivatives were done with the bootstrap method.

Sizes studied were $L = 4,6,8,12,16,24,32,48,64,96$, and 128 for both Gaussian and bimodal interactions, with $2^{13} = 8192$ samples (J_{ij} interactions) for each size.

III. SPECIFIC HEAT

The size dependence of the ground-state energy per spin $e(0,L)$ for the 2D Gaussian ISG has been shown [14,22] to follow the simple critical finite-size scaling rule

$$e(0,L) - e(0,\infty) \sim L^{2-\theta}, \quad (4)$$

with a θ consistent with the estimate from ground-state domain wall stiffness measurements [1]. Standard scaling arguments [4] would suggest that the low-temperature specific heat should behave as

$$C_v(\beta,L) \sim \beta^{-2\nu} \approx \beta^{-7}, \quad (5)$$

but because of the continuous interaction distribution, in addition to critical excitations there are always single spin excitations. These lead to a term $C_v(\beta,L) \approx T$ which dominates the Gaussian low-temperature specific heat as noted by Ref. [4]. Specific heat data for the bimodal model were calculated through the present simulations; data extending to a much lower temperature range and larger sizes have already been measured using the sophisticated Pfaffian arithmetic technique by Lukic *et al.* [4] and by Thomas *et al.* [5], and we are very grateful to be able to quote these results *in extenso*.

The data for the two models are shown (see Figs. 1 and 2) in the form of plots of the derivative $y = \partial \ln[C_v(\beta,L)]/\partial\beta$ against $x = T$. This nonconventional form of plot happens to

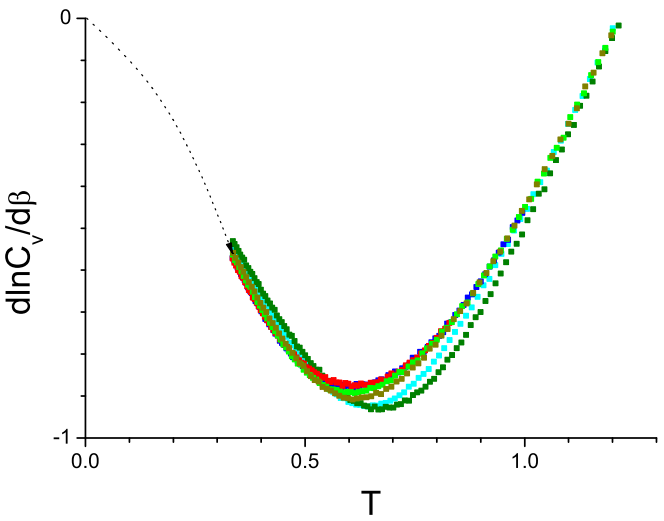

FIG. 1. Gaussian 2D ISG. Logarithmic derivative of the specific heat $\partial \ln C_v(T,L)/\partial\beta$ against T. Sizes $L = 64,48,32,24,16,12$ top to bottom in the dip. Curve: extrapolation.

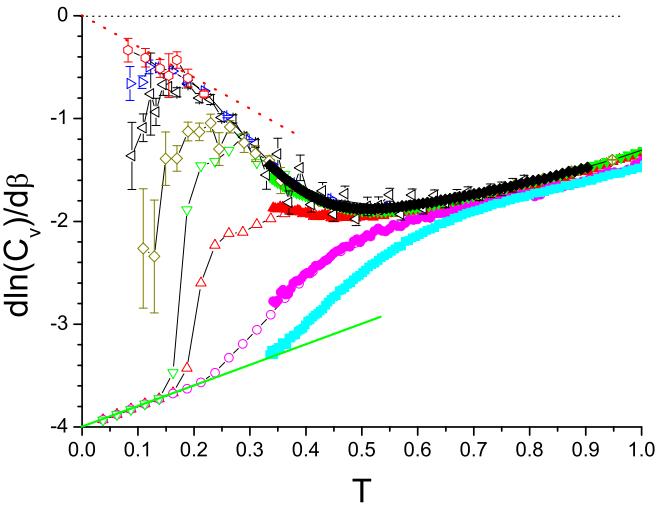

FIG. 2. Bimodal 2D ISG. Logarithmic derivative of the specific heat $\partial \ln C_v(T,L)/\partial\beta$ against T. Full points: simulation data $L = 96,48,24,12,8$ (black, green, red, pink, cyan) top to bottom. Open points: Pfaffian data; red polygons $L = 512$, blue right triangles $L = 256$, black left triangles $L = 128$, brown diamonds $L = 64$ (all data from Ref. [5]), green down triangles $L = 50$, red up triangles $L = 24$, pink circles $L = 12$, all data from Ref. [4]. Dashed diagonal red line $y = -3x$, green diagonal line $y = -4 + 2x$.

be particularly instructive. A low-temperature limit $C_v(\beta,L) \sim T^x$ appears as a straight line through the origin with slope $-x$, while a low-temperature limit of the "naive" bimodal ground-state-dominated form Eq. (1) appears as a straight line with intercept -4 and slope $+2$.

The Gaussian data are almost independent of L for the whole temperature range. Physically this occurs because the specific heat in ISGs is predominately a near-neighbor effect. The curve tends to a slope $\partial y/\partial x \sim -1$ corresponding to $C_v \sim T^1$ in the low-T limit, in agreement with the conclusion of Ref. [3].

For the bimodal model there is first a high-temperature and/or high-L envelope curve corresponding to the effectively continuous $T > T^*(L)$ regime. In this regime finite-size effects are very weak: the specific heat is almost independent of L as in the Gaussian. The curves for the two models are of similar form but are not identical. In the large L, the low-T limit of this envelope curve, the bimodal data as shown in Fig. 2 indicate $C_v \sim T^3$, in agreement with the conclusions drawn in Ref. [5] based on droplet excitation arguments.

For each L the data curve peels off the large-L envelope curve below an L-dependent temperature, which can be identified with the start of the effectively continuous to ground-state-dominated regime crossover centered at $T^*(L)$. Finally, for each L in the low-temperature range $T \ll T^*(L)$ the specific heat links up to the "naive" limit of Eq. (1). (It should be noted that because of the logarithmic derivative, temperature-independent L-dependent factors do not show up in this plot.) The crossover can be seen to be gentle for small L, becoming sharp for large L. Defining $T^*(L)$ as the location of the maximum positive slope on this plot, the crossover temperatures can be clearly identified and are consistent with $T^*(L)L^{1/2} = 1.1(1)$, in agreement with the prediction of Ref. [5].

An anomalous limit of the form

$$C_v(\beta) \sim \beta^2 \exp(-2\beta), \tag{6}$$

which has been proposed by some authors [4,23] following Ref. [24], is inconsistent with the data in Fig. 2 for all L and T (see also [25,26]). An intermediate L regime where $C_v(\beta,L) \sim T^{5.25}$, as proposed in Ref. [16], or $C_v(\beta,L) \sim T^{4.2}$, as proposed in Ref. [15], appears to be valid only for a limited range of T and L.

IV. THE EXPONENT η

For ISGs with nonzero critical temperatures, finite-size scaling analyses at and close to the critical temperature are used to estimate critical exponents. For the 2D bimodal ISG, because of the crossover to the ground-state-dominated regime, this approach is ruled out and the critical exponents must be estimated using the entirely different strategy of ThL measurements.

The standard renormalization group theory (RGT) scaling variable for models with nonzero ordering temperatures is $t = (T - T_c)/T_c$. This obviously cannot be used when $T_c = 0$; by convention the scaling variable used in the literature for 2D ISGs is the un-normalized temperature T. This is only a convention; it is perfectly legitimate to use other conventions. Thus, when considering the canonical one-dimensional (1D) Ising ferromagnet, Baxter [27] remarks, "When $T_c = 0$ it is more sensible to replace $t = (T - T_c)/T_c$ by $\tau = \exp(-2\beta)$." (In fact, for the particular 1D model, scaling without corrections over the entire temperature range follows if a related scaling variable $\tau = 1 - \tanh(\beta)$ is chosen [28,29].) Below we will introduce another scaling variable appropriate for ISGs with $T_c = 0$, but for the moment we follow this traditional $t = T$ 2D ISG convention. The critical exponents are defined through the leading ThL expressions for the reduced susceptibility and the second moment correlation length within this convention: $\chi(T) = C_\chi T^{-(2-\eta)\nu}$ and $\xi(T) = C_\xi T^{-\nu}$ in the limit $T \to 0, L \to \infty$. For all data which fulfill the condition (either in the bimodal and Gaussian models) $L > K\xi(T,L)$ with $K \approx 6$, observables such as $\chi(T,L)$ and $\xi(T,L)$ depend on T but not on L, and so correspond to the ThL infinite size values $\chi(T)$ and $\xi(T)$. The ThL condition defines implicitly a crossover temperature $T_\xi(L)$. It turns out that in the bimodal 2D ISG the ThL limit temperature $T_\xi(L)$ is always higher than the corresponding crossover temperature to the ground-state-dominated regime $T^*(L)$ defined above, so the ThL data are always well within the effectively continuous regime. The ThL data extrapolation to $T = 0$ corresponds to estimates for the critical exponents in the successive limits $[L \to \infty, T \to 0]$ and so in the effectively continuous energy level regime, to be distinguished from the exponents defined taking the successive limits $[T \to 0, L \to \infty]$, which would correspond to the "finite-size" ground-state-dominated regime.

There have been many previous studies having the aim of estimating the critical exponents and in particular, η for the bimodal model. McMillan already in 1983 estimated $\eta = 0.28(4)$ from the $G(r)$ correlation data on one $L = 96$ sample well in the effectively continuous regime [18]. Katzgraber

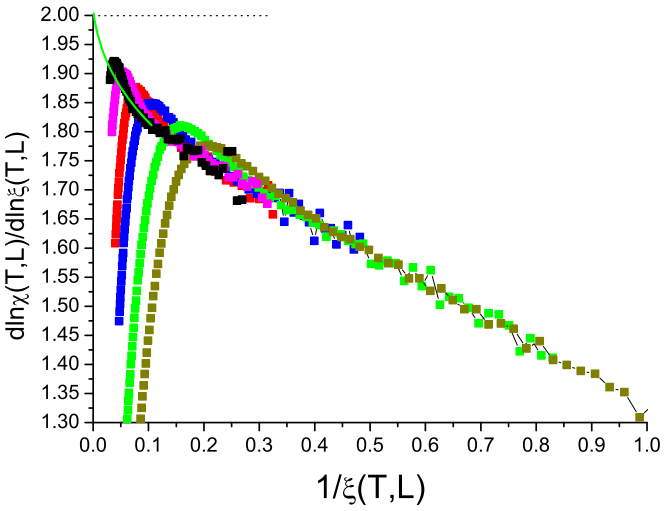

FIG. 3. Gaussian 2D ISG. Derivative $\partial \ln \chi(T,L)/\partial \ln \xi(T,L)$ against $1/\xi(T,L)$ for $L = 128,96,64,48,32,24$ left to right. In this and all following figures both Gaussian and bimodal, the color coding is black, pink, red, blue, green, brown, cyan, olive for $L = 128,96,64,48,32,24,16,12$.

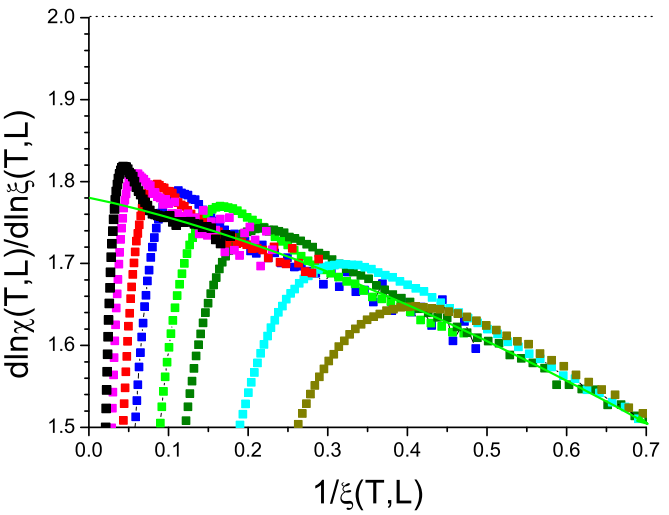

FIG. 4. Bimodal 2D ISG. Derivative $\partial \ln \chi(T,L)/\partial \ln \xi(T,L)$ against $1/\xi(T,L)$ for $L = 128,96,64,48,32,24$ left to right. Same color coding as in Fig. 3.

and Lee [20] estimated $\eta = 0.138(5)$ from $\chi(T,L)$ data. Jörg *et al.* [3] show a plot of $\ln \chi(T)$ against $\ln \xi(T)$ after an extrapolation to infinite L using the technique of Ref. [30]. They state "fits of this curve lead to values of η that are very small, between 0 and 0.1, strongly suggestive of $\eta = 0$." However, this type of extrapolation to infinite L is delicate, particularly in the bimodal 2D case.

In addition, the data displayed by [3] on a $\ln \chi(T) - \ln \xi(T)$ plot extending over five decades on the y axis are hard to fit with precision. Katzgraber *et al.* [15] show a plot of $\partial \ln \chi(T,L)/\partial \ln \xi(T,L)$ which in principle is equivalent to the Ref. [3] plot but which provides a display much more sensitive to the value of η; they state cautiously, "for all system sizes and temperatures studied $\eta_{\rm eff}$ is always greater than 0.2, although an extrapolation to $\eta = 0$ cannot be ruled out," so that the possibility of the bimodal and Gaussian ISGs being in the same universality class "cannot be reliably proven." In Refs. [31] and [32] it is claimed that the Gaussian and bimodal models are in the same universality class, which is surprising as "the data are not sufficiently precise to provide a precise determination of η, being consistent with a small value $\eta \leqslant 0.2$, including $\eta = 0$."

All the estimates quoted so far can be considered to concern the effectively continuous regime. At zero or low temperatures, so in the ground-state-dominated regime, different sophisticated algorithms lead to the estimates $\eta = 0.14(1)$ [13], and to $\eta = 0.22$ [17].

In Figs. 3 and 4, we show plots of $y(x) = \partial \ln \chi(T,L)/\partial \ln \xi(T,L)$ against $x = 1/\xi(T,L)$ for the Gaussian and bimodal models. These are *raw* data points having the high statistical precision of the present measurements. With the conventional definition of the critical exponents through $\chi(T,L) \sim T^{-(2-\eta)\nu}$ and $\xi(T,L) \sim T^{-\nu}$ in the ThL regime low-T limit, the limiting slope $\partial y/\partial x$ at criticality as $x \to 0$ is by definition equal to $2 - \eta$. For the Gaussian model the observed tendency of the low-T slope with increasing L is consistent with the limit value $\eta = 0$, which must be the case for this nondegenerate ground-state model. For the bimodal model the observed $y(x)$ in the ThL regime is not tending to 2 with increasing L but to a constant limit of 1.78(2). Slight overshoots for each L in both systems can be ascribed to $\chi(T,L)$ and $\xi(T,L)$ not reaching the ThL condition at quite the same temperature. As stated above, very similar observations were made in Ref. [15] for the bimodal model. The present results thus confirm unambiguously that for the bimodal ISG in the effectively continuous regime η is not zero but is $\approx$0.20(2). Thus the bimodal ISG in the effectively continuous ThL regime and the Gaussian ISG are not in the same universality class. The present authors have published evidence for nonuniversal scaling in dimension-4 Ising spin glasses also [33]. Measurements have also been published on the bimodal Migdal-Kadanoff model in dimension 2 [34].

V. SCALING AND ZERO-TEMPERATURE ORDERING

Estimating the remaining exponent ν [or $\gamma = (2 - \eta)\nu$] is more difficult than for the exponent η. As we have noted above, the standard RGT convention for models with finite temperature ordering is to use the scaling variable $t = (T/T_c) - 1$, which obviously cannot be applied to models with $T_c = 0$, and for 2D ISGs the preferred convention in the literature has been to use the un-normalized scaling variable $t = T$. In practice this is inefficient, as the extrapolations towards the $T = 0$ limit in order to estimate the value of the critical exponent ν are very ambiguous. For instance, when presenting T-scaled susceptibility data for sizes up to $L = 128$, Katzgraber *et al.* [15] state "the [susceptibility] data for the bimodal case can be extrapolated to any arbitrary value including $1/\gamma_{\rm eff} = 0$."

We introduce a novel scaling variable suitable for the 2D ISGs, applying the same principles as for ISGs at higher dimensions [6], adapted to $T = 0$ ordering:

(i) For spin glasses the relevant interaction strength parameter is not J but is $\langle J^2 \rangle$, so the natural dimensionless

parameter is $\langle J^2\rangle\beta^2$ [or alternatively, $\tanh^2(J\beta)$ for bimodal ISGs]. With the standard normalization $\langle J^2\rangle = 1$ the natural inverse "temperature" in ISGs is β^2, not β. This was recognized immediately after the Edwards-Anderson model was introduced, in high-temperature series expansion (HTSE) analyses for ISGs including 2D models [35–37], but has since been overlooked in most simulation analyses.

(ii) It is convenient to choose a scaling variable τ defined in such a way that $\tau = 0$ at criticality and $\tau = 1$ at infinite temperature. With an ISG ordering at a finite inverse temperature β_c, $\tau(\beta) = 1 - \beta^2/\beta_c^2$ is an appropriate choice [6,37]. When $\beta_c = \infty$ as in the 2D ISG case, $\tau_t(\beta) = 1 - [\tanh(\beta)/\tanh(\beta_c)]^2 = 1 - \tanh(\beta)^2$ has been used [35], but here we prefer $\tau_b(\beta) = 1/(1+\beta^2)$, as it turns out to be efficient and the limits are easy to relate to those of the T-scaling convention. With nonzero T_c the effective exponents at criticality do not depend on the choice of scaling variable; this is not the case when $T_c = 0$, but a simple dictionary is given below relating the limiting derivatives for τ_b scaling to the exponents for the conventional T scaling.

(iii) The ThL HTSE Darboux [38] format for observables $Q(x)$ is

$$Q(x) = 1 + a_1 x + a_2 x^2 + a_3 x^3 + \cdots, \tag{7}$$

with $x = \beta^2$ in ISGs [37]. The HTSE ISG susceptibility $\chi(\beta^2)$ is naturally in this format, so for ISG models with $T_c > 0$ the ThL susceptibility can be scaled in the Wegner [39] form

$$\chi(\beta^2) = C_\chi \tau(\beta^2)^{-(2-\eta)\nu} F[1 + a_\chi \tau(\beta^2)^\theta + \cdots]. \tag{8}$$

Because the correlation function second moment μ_2 HTSE is of the form (see Ref. [40] for the Ising ferromagnet)

$$\mu_2(x) = x + a_1 x^2 + a_2 x^3 + \cdots \tag{9}$$

and the second moment correlation length is defined through $\xi(x)^2 = \mu_2/[z\chi(x)]$, with z the number of nearest neighbors, for consistency the appropriate correlation length variable for ISG scaling is $\xi(x)/\beta$ rather than $\xi(x)$ (whether T_c is zero or not). This point has been spelled out in Ref. [6].

Examples of applications of the scaling rules outlined here to other specific models (both ferromagnets and ISGs) have been given elsewhere. A general discussion of ferromagnets and spin glasses is given in Ref. [6], analyses of 3D Ising, XY, and Heisenberg ferromagnets in Ref. [41], the 2D Ising ferromagnet is analyzed in Ref. [42], 3D Ising ferromagnets in [29,43], high-dimension Ising ferromagnets in Ref. [44], and the 2D Villain fully frustrated model in Ref. [28].

The scaling of the Binder cumulant

$$g(\beta^2) = \frac{1}{2}\left(3 - \frac{[\langle q^4\rangle]}{[\langle q^2\rangle]^2}\right) \tag{10}$$

is discussed in Appendix A. The 2D simulation data analysis and the extrapolations below are based on the derivatives $\partial \ln Q(\tau_b, L)/\partial \ln \tau_b$ in the ThL regime where these derivatives are independent of L and so are equal to the infinite size derivatives. An advantage of the 2D models is that in contrast to $\tau(\beta^2)$ for the models with nonzero T_c, for the 2D ISGs with $T_c \equiv 0$ there is no uncertainty in the definition of $\tau_b(\beta^2)$ related to an uncertainty in the value of the ordering temperature.

Once the $\tau_b \to 0$ limits for the various derivatives have been estimated by extrapolation of the ThL data for finite L, there is a simple dictionary for translating into terms of the conventional T-scaling critical exponents ν and η defined above:

$$-\frac{\partial \ln \chi(\tau_b)}{\partial \ln \tau_b} \to \frac{\nu(2-\eta)}{2}, \tag{11a}$$

$$-\frac{\partial \ln[T\xi(\tau_b)]}{\partial \ln \tau_b} \to \frac{(\nu-1)}{2}, \tag{11b}$$

$$\frac{\partial \ln \chi(\tau_b)}{\partial \ln[T\xi(\tau_b)]} \to \frac{\nu(2-\eta)}{\nu-1}, \tag{11c}$$

$$-\frac{\partial \ln g(\tau_b)}{\partial \ln \tau_b} \to \nu. \tag{11d}$$

VI. ANALYSES WITH THE SCALING VARIABLE τ_b

The four derivatives of Eq. (11) are shown in Figs. 5–12. In contrast to the derivatives in which T is used as the scaling variable, each derivative can be extrapolated in a fairly unambiguous manner to criticality as discussed below; there is always an exact finite value at infinite temperature $\tau_b = 1$.

The exact infinite temperature limits from the general high-temperature scaling expansion expressions [37] applied to scaling with τ_b are (when $\tau_b \to 1$)

$$-\frac{\partial \ln \chi(\tau_b)}{\partial \ln \tau_b} = 4\,(\text{Gauss.}), \ldots = 4\,(\text{bimodal}), \tag{12a}$$

$$\frac{\partial \ln[T\xi(\tau_b)]}{\partial \ln \tau_b} = 1\,(\text{Gauss.}), \ldots = \frac{5}{3}\,(\text{bimodal}), \tag{12b}$$

$$\frac{\partial \ln \chi(\tau_b)}{\partial \ln[T\xi(\tau_b)]} = 4\,(\text{Gauss.}), \ldots = \frac{12}{5}\,(\text{bimodal}). \tag{12c}$$

The method used for extrapolation to criticality is through polynomial fits and is outlined in Appendix B. With $\eta = 0$ and assuming $\nu = 3.55(5)$ [8], the predicted Gaussian critical

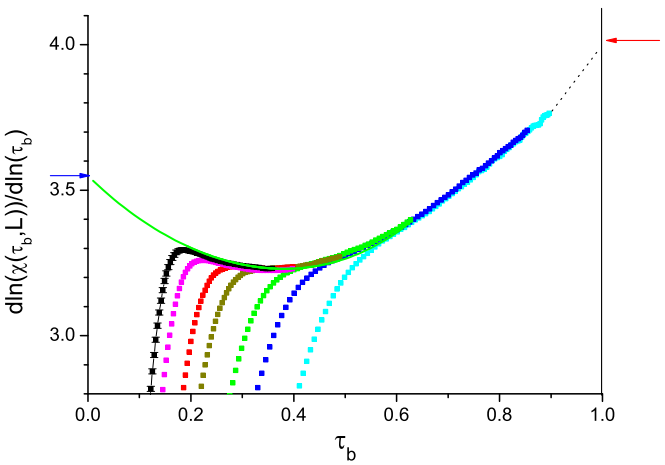

FIG. 5. Gaussian 2D ISG. The derivative $\partial \ln \chi(T,L)/\partial \ln \tau_b$ against τ_b. Sizes $L = 128,96,64,48,32,24,16$ left to right. Same color coding as in Fig. 3. Dashed line: extrapolation. Red arrow: exact infinite temperature value. Blue arrow: Gaussian critical value.

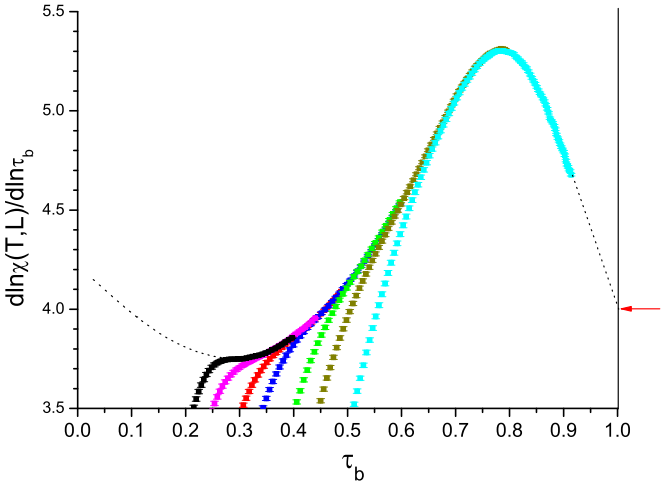

FIG. 6. Bimodal 2D ISG. The derivative $\partial \ln \chi(T,L)/\partial \ln \tau_b$ against τ_b. Sizes $L = 128,96,64,48,32,24,16$ left to right. Same color coding as in Fig. 3. Dashed line: extrapolation. Red arrow: exact infinite temperature value.

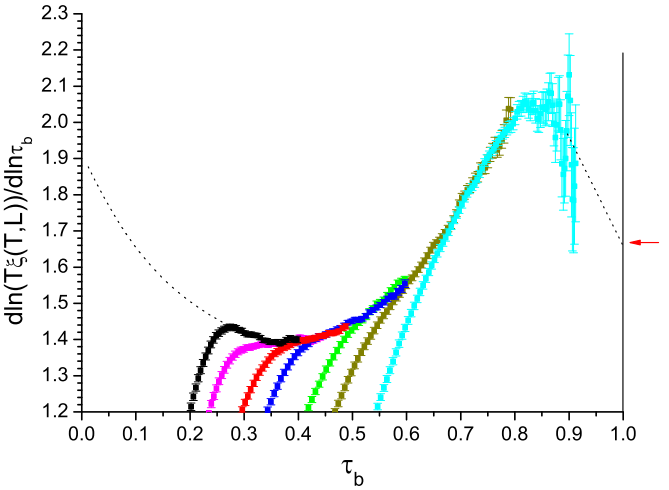

FIG. 8. Bimodal 2D ISG. The derivative $\partial \ln[T\xi(T,L)]/\partial \ln \tau_b$ against τ_b. Sizes $L = 128,96,64,48,32,24,16$ left to right. Same color coding as in Fig. 3. Dashed line: extrapolation. Red arrow: exact infinite temperature value.

limits (when $\tau_b \to 0$) for the derivatives are

$$-\frac{\partial \ln \chi(\tau_b)}{\partial \ln \tau_b} \to 3.55(5), \tag{13a}$$

$$-\frac{\partial \ln[T\xi(\tau_b)]}{\partial \ln \tau_b} \to 1.28(3), \tag{13b}$$

$$\frac{\partial \ln \chi(\tau_b)}{\partial \ln[T\xi(\tau_b)]} \to 2.78(1), \tag{13c}$$

$$-\frac{\partial \ln g(\tau_b)}{\partial \ln \tau_b} \to 3.55(3). \tag{13d}$$

From the fitted ThL data extrapolations (see Figs. 5, 7, 9, 11, and Appendix B) the estimated Gaussian critical limit values (the estimated intercepts from the fits) are 3.40(10),1.28(5),2.76(10),3.6(1), respectively. These values are fully consistent with the list above, which validates the polynomial extrapolation procedure that we have used, even though it must be kept in mind that it is only an efficient approximation. Ideally the extrapolation should be made through invoking Wegner correction terms [39], but this requires having information on the correction exponents which are *a priori* unknown. In Appendix B we outline an estimation of the leading correction exponent θ from the data for the most favorable Gaussian case available. It turns out that $\theta = 1$ appears to be a good estimate, which provides some fundamental backing to the polynomial fit approach.

The bimodal ThL data are extrapolated to criticality using just the same protocol as used in the Gaussian data. For the

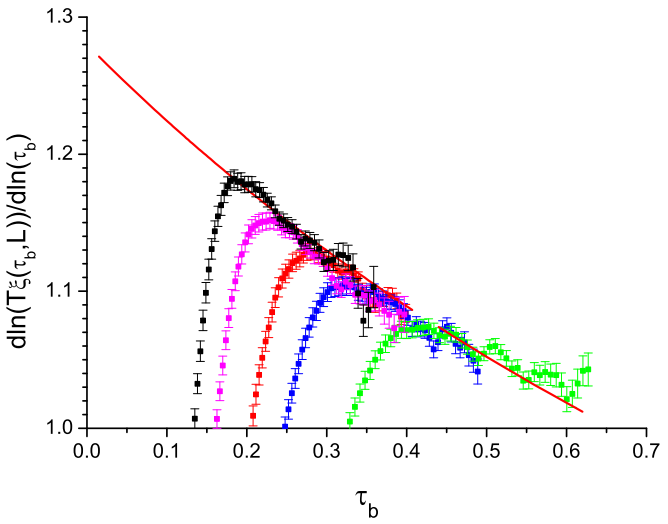

FIG. 7. Gaussian 2D ISG. The derivative $\partial \ln[T\xi(T,L)]/\partial \ln \tau_b$ against τ_b. Sizes $L = 128,96,64,48,32,24$ left to right. Same color coding as in Fig. 3. Red curve: fit.

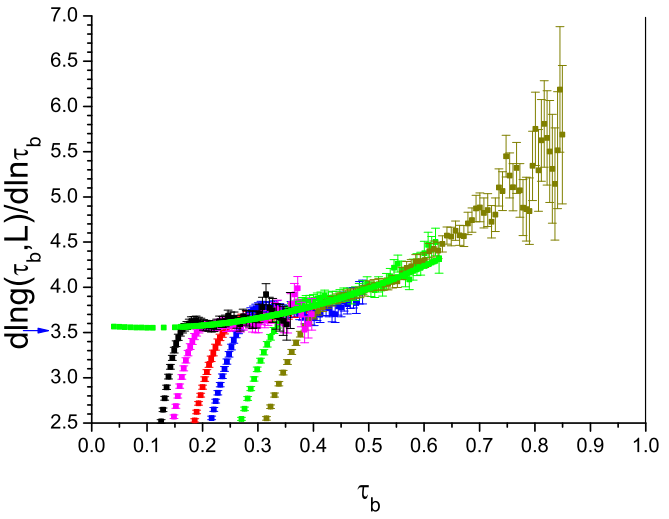

FIG. 9. Gaussian 2D ISG. The derivative $\partial \ln g(T,L)/\partial \ln \tau_b$ against τ_b, where $g(T,L)$ is the Binder cumulant. $L = 128,96,64,48,32,24$ left to right. Same color coding as in Fig. 3. Green curve: fit.

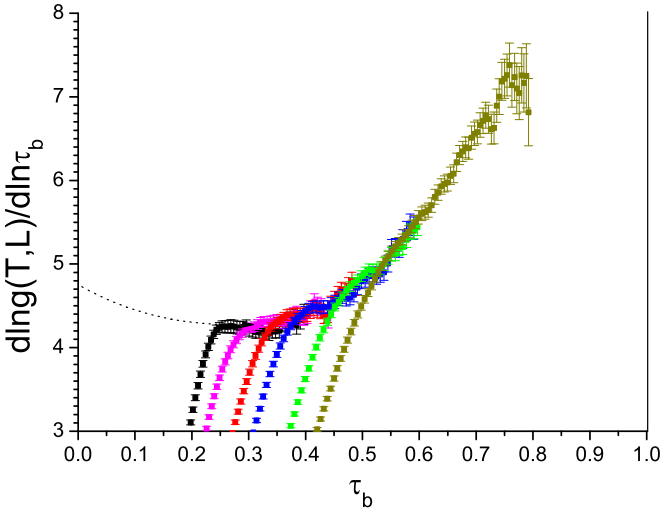

FIG. 10. Bimodal 2D ISG. The derivative $\partial \ln g(T,L)/\partial \ln \tau_b$ against τ_b, where $g(T,L)$ is the Binder cumulant. Sizes $L =$ 128,96,64,48,32,24 left to right. Same color coding as in Fig. 3. Dashed line: extrapolation.

bimodal model, the extrapolated ThL limits (when $\tau_b \to 0$) from the figures (see Appendix B) give the following estimates:

$$-\frac{\partial \ln \chi(\tau_b)}{\partial \ln \tau_b} \to 4.3(1), \tag{14a}$$

$$-\frac{\partial \ln[T\xi(\tau_b)]}{\partial \ln \tau_b} \to 1.9(1), \tag{14b}$$

$$\frac{\partial \ln \chi(\tau_b)}{\partial \ln[T\xi(\tau_b)]} \to 2.15(10), \tag{14c}$$

$$-\frac{\partial \ln g(\tau_b)}{\partial \ln \tau_b} \to 4.8(3). \tag{14d}$$

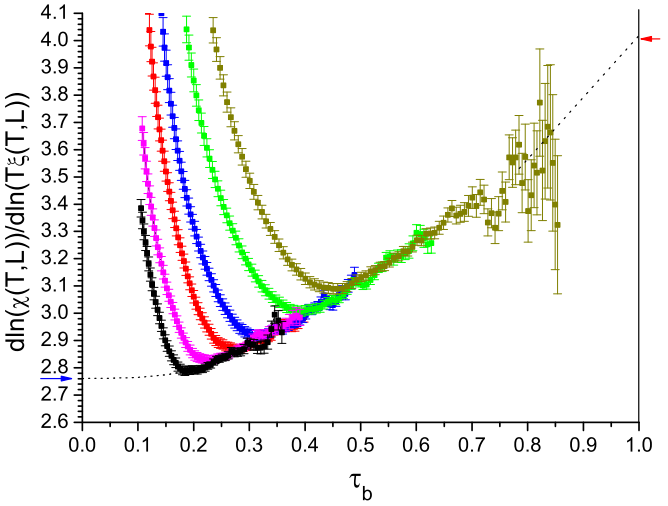

FIG. 11. Gaussian 2D ISG. The derivative $\partial \ln \chi(T,L)/\partial \ln[T\xi(T,L)]$ against τ_b. Sizes $L =$ 128,96,64,48,32,24 left to right. Same color coding as in Fig. 3. Dashed line: extrapolation. Red arrow: exact infinite temperature value. Blue arrow: Gaussian critical value.

Each of these estimated critical intercepts is significantly different from the analogous Gaussian value. When translated into the T-scaling convention, and with $\eta = 0.20(2)$ (see Sec. IV), the four 2D bimodal critical intercept estimates from these measurements are consistent with $\nu = 4.8(3)$ [so $\gamma = (2-\eta)\nu = 8.6(5)$]. Thus not only is the ThL bimodal exponent η different from the Gaussian value, but the estimated bimodal value of the exponent ν is different from the Gaussian value also. It should be noted that ground-state bimodal droplet calculations [17] lead to $\eta \approx 0.22$ and $\nu_{dp} \approx 3.5$.

VII. CONCLUSION

Simulation data are presented for the canonical Gaussian and bimodal interaction distribution Ising spin glasses in dimension 2, which is known to order only at zero temperature. For both models simulations were carried out for different sample sizes up to a maximum size $L = 128$, with 8192 samples at each size. In order to facilitate extrapolations to zero temperature, a temperature scaling variable $\tau_b = T^2/(1+T^2)$ is introduced in addition to the conventional 2D ISG unnormalized scaling variable $t = T$. Extrapolations to criticality for different observables were made using polynomial fits.

The bimodal specific heat simulation data supplemented by data from Lukic *et al.* [4] and from Thomas *et al.* [5] show clear crossovers from an effectively continuous energy level thermodynamic limit regime to a finite-size ground-state-dominated regime at size-dependent temperatures $T^*(L) \approx 1.1/L^{1/2}$ (see Ref. [5]).

The Gaussian thermodynamic limit simulation data extrapolated to criticality using τ_b scaling and polynomial fits lead to estimates for the critical intercepts which are completely consistent with the well-established critical exponents for this model, which are $\eta \equiv 0$ and $\nu = 3.55(5)$ [8] when expressed in terms of the conventional scaling variable $t = T$.

The bimodal thermodynamic limit simulation results were analyzed in two alternative ways. Using the conventional scaling approach, the derivative $\partial \ln \chi(T,L)/\partial \ln \xi(T,L)$ plotted against $1/\xi(T,L)$ (Fig. 4) shows a critical value which corresponds to $\eta = 0.20(2)$, so strictly nonzero and very similar to the $T = 0$ value $\eta \approx 0.22$ estimated quite independently from exact ground-state calculations [17]. The bimodal simulation data for four different observables are plotted using the τ_b scaling in Figs. 6, 8, 10, and 12. The bimodal critical intercepts estimated from extrapolations of the thermodynamic limit data made using just the same protocol as for the Gaussian model are all significantly different from the Gaussian intercepts (see figures in Appendix B). Translated into terms of the conventional $t = T$ scaling, the bimodal intercept values correspond consistently to critical exponents $\eta = 0.20(2)$ and $\nu = 4.8(3)$, clearly distinct from the Gaussian values. The conclusion that the 2D bimodal and Gaussian ISGs are not in the same universality class appears to be on very firm ground, but data to still higher L would be welcome. It should be possible to consider the issue completely closed when data to much higher L (say perhaps to $L = 256$) becomes available. This would require a considerable numerical effort in order to attain equilibrium to still lower temperatures on these large samples.

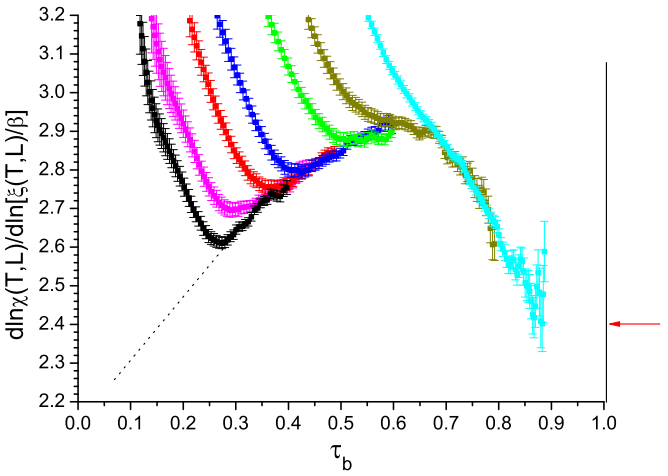

FIG. 12. Bimodal 2D ISG. The derivative $\partial \ln \chi(T,L)/\partial \ln[T\xi(T,L)]$ against τ_b. Sizes $L = 128,96,64,48,32,24,16$ left to right. Same color coding as in Fig. 3. Dashed line: extrapolation. Red arrow: exact infinite temperature value.

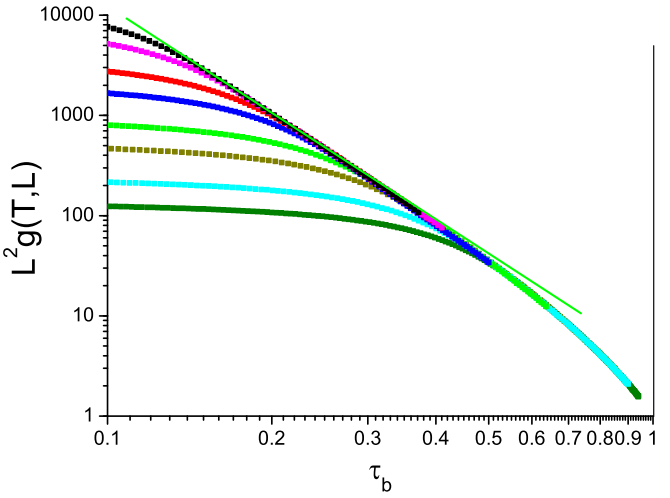

FIG. 13. Gaussian 2D ISG. $L^2 g(\tau_b)$ against τ_b. Sizes $L = 128,96,64,48,32,24,16,12$ top to bottom. Same color coding as in Fig. 3. $g(T,L)$ is the Binder cumulant. Line slope -3.5.

ACKNOWLEDGMENTS

We are very grateful to Olivier Martin and to Alan Middleton who generously allowed us access to the specific heat data of Refs. [4] and [5], respectively. We would like to thank Alex Hartmann for very helpful suggestions. The computations were performed on resources provided by the Swedish National Infrastructure for Computing (SNIC) at the High Performance Computing Center North (HPC2N) and Chalmers Centre for Computational Science and Engineering (C3SE).

APPENDIX A: BINDER CUMULANT

The ferromagnetic Binder cumulant has been extensively exploited in the finite-size scaling limit regime very close to criticality for its properties as a dimensionless observable. In addition, its ThL properties can also be studied. In Ising ferromagnets, the critical exponent for the second field derivative of the susceptibility χ_4 (also called the nonlinear susceptibility) is [40]

$$\gamma_4 = \gamma + 2\Delta = \nu d + 2\gamma. \tag{A1}$$

The nonlinear susceptibility χ_4 is directly related to the Binder cumulant [45], Eq. (10.2), through

$$g(\beta,L) = \frac{-\chi_4}{L^d \chi^2} = \frac{3\langle m^2\rangle - \langle m^4\rangle}{\langle m^2\rangle^2}. \tag{A2}$$

As χ scales with the critical exponent γ, the normalized Binder cumulant $L^d g(\beta,L)$ scales with the ThL regime critical exponent $\partial \ln(L^d g)/\partial \ln \tau = (\nu d + 2\gamma) - 2\gamma = \nu d$. In any $S = 1/2$ Ising system the infinite temperature (independent spin) limit for the Binder cumulant is

$$g(\infty,N) \equiv 1/N, \tag{A3}$$

where N is the number of spins; $N = L^d$ for a hypercubic lattice. So $L^d g(\beta,L)$ has an infinite temperature limit which is strictly 1, and a large-L critical limit (with corrections as for the other observables) of

$$L^d g(\tau_b,L) \sim \tau_b^{-\nu d}(1 + \cdots). \tag{A4}$$

Exactly the same argument can be transposed to ISGs (see Ref. [36] for χ_4 in ISGs). In the particular case of a 2D ISG model with τ_b scaling, the critical value for the derivative $\partial \ln[L^d g(\tau_b,L)]/\partial \ln \tau_b$ of the Binder cumulant ThL data extrapolated to $\tau_b = 0$ is $2\nu/2 = \nu$, where ν is once again the correlation length critical exponent in the T-scaling convention. The Binder cumulant data plotted in the Eq. (A4) form are shown for the two models in Figs. 13 and 14. The ThL envelope curves can be seen by inspection. The derivatives of these curves have already been shown in Figs. 9 and 10.

It has been suggested that if two models have the same function when $y = g(\beta,L)$ is plotted against $x = \xi(\beta,L)/L$, it is a proof of universality. However, because both $Lg^{1/d}(\beta,L)$

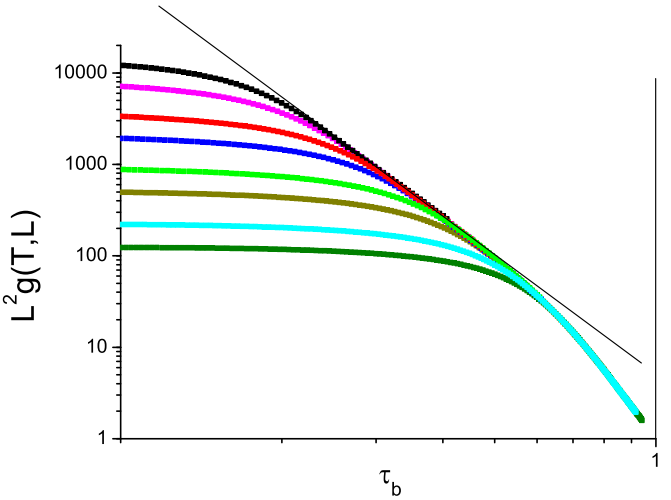

FIG. 14. Bimodal 2D ISG. $L^2 g(\tau_b)$ against τ_b. Sizes $L = 128,96,64,48,32,24,16,12$ top to bottom. Same color coding as in Fig. 3. $g(T,L)$ is the Binder cumulant. Line slope -4.2.

and $\xi(\beta, L)$ are controlled by just the same exponent ν, this is questionable.

APPENDIX B

As the data sets do not extend to infinite size, to estimate the critical $\tau_b = 0$ limit values from the ThL derivative data in Figs. 5–12, an extrapolation must be made. There is no definitive method to extrapolate so as to be sure to obtain exact values of the critical exponents, though data to still larger sizes would make the task easier. The most economical choice for extrapolation is to assume that the ThL derivative data continue to evolve smoothly and regularly when an extrapolation is made towards $\tau_b = 0$ through the smaller τ_b region where no ThL data are for the moment available. To do this, for each derivative observable $y(x)$ with $x = \tau_b$ we collect together the ThL data points for all the sizes L up to $x = 0.6$ and make standard polynomial fits with 3 or 4 terms:

$$y(x) = a_0 + a_1 x + a_2 x^2 \tag{B1}$$

or

$$y(x) = a_0 + a_1 x + a_2 x^2 + a_3 x^3. \tag{B2}$$

(In fits with larger numbers of terms the fit parameter values become unstable.) Assuming that each polynomial fit curve extended to $\tau_b = 0$ is a good approximation to the true behavior, each a_0 is an estimate for the critical limit value. The a_0 values for three or four parameter fits turn out to be similar. In Figs. 15, 16, 17, and 18 the data and fits are shown for $\partial \ln \chi(\tau_b)/\partial \ln \tau_b$, $\partial \ln[T\xi(\tau_b)]/\partial \tau_b$, $\partial \ln \chi(\tau_b)/\partial \ln[T\xi(\tau_b)]$, and $\partial \ln g(\tau_b)/\partial \ln \tau_b$ for both Gaussian and bimodal models. The fits are automatic, so this procedure is objective and we assume that it is optimal for the available data. All the Gaussian extrapolated critical values estimated in this way are close to those expected assuming the published exponents, $\eta = 0$ and $\nu = 3.55(5)$ [8]. This implies that the estimated bimodal critical values should also be trustworthy. Inspection of Figs. 6 and 8 shows that having the $L = 128$ data in hand is useful for pinning down the extrapolated intercepts more precisely. However, including or excluding the $L = 128$ data sets when making the fits does not change the intercept estimates by more than a few percent.

Though the polynomial extrapolations are plausible, objective, and precise, they may seem rather arbitrary. A more fundamental approach would invoke correction terms with Wegner thermal correction exponents [39]. Unfortunately, the values of the effective leading and subleading correction exponents are *a priori* unknown and hard to determine, even in ferromagnets which are much simpler than ISGs. However, consider the particular case of the 2D Gaussian

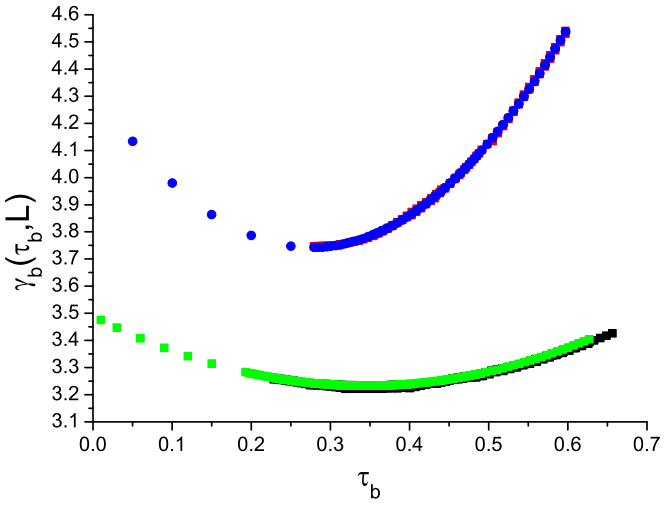

FIG. 15. The ThL $\partial \ln \chi(\tau_b)/\partial \ln \tau_b$ data for the Gaussian model from Fig. 5 (lower, black, squares) with the polynomial fit (lower, green, circles, smooth), and for the bimodal model from Fig. 6, (upper, red, squares) with the polynomial fit (upper, blue, circles, smooth).

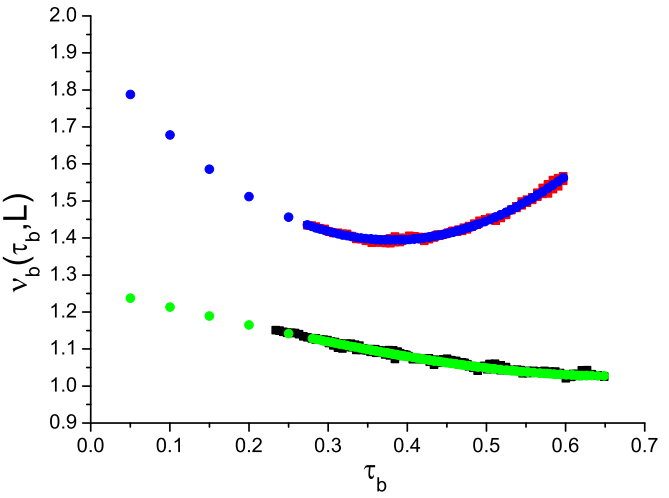

FIG. 16. The ThL $\partial \ln[T\xi(\tau_b)]/\partial \ln \tau_b$ data for the Gaussian model from Fig. 7 (lower, black, squares) with the polynomial fit (lower, green, circles, smooth), and for the bimodal model from Fig. 8 (upper, red, squares) with the polynomial fit (upper, blue, circles, smooth).

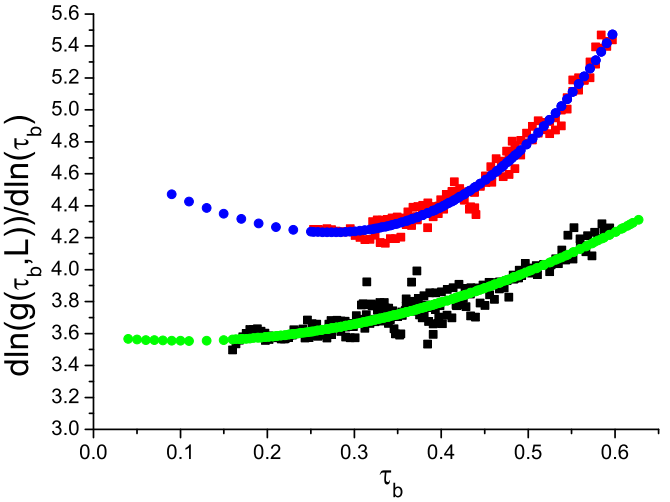

FIG. 17. The ThL $\partial \ln g(\tau_b)/\partial \ln \tau_b$ data for the Gaussian model from Fig. 9 (lower, black, squares) with the polynomial fit (lower, green, circles, smooth), and for the bimodal model from Fig. 10 (upper, red, squares) with the polynomial fit (upper, blue, circles, smooth).

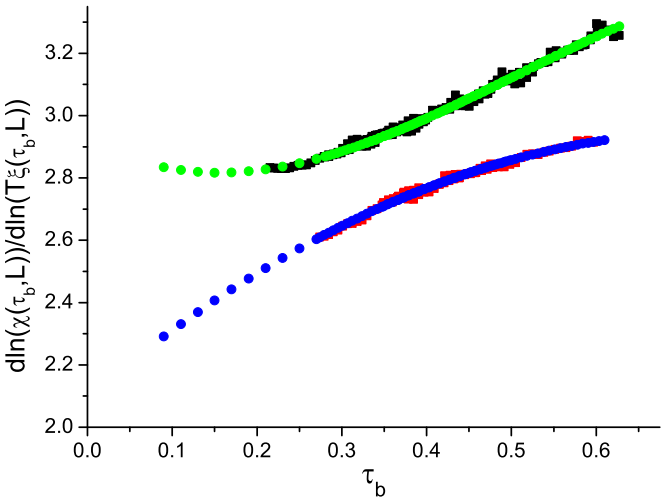

FIG. 18. The ThL $\partial \ln \chi(\tau_b)/\partial \ln[T\xi(\tau_b)]$ data for the Gaussian model from Fig. 11 (upper, black, squares) with the polynomial fit (upper, green, circles, smooth), and for the bimodal model from Fig. 12 (lower, red, squares) with the polynomial fit (lower, blue, circles, smooth).

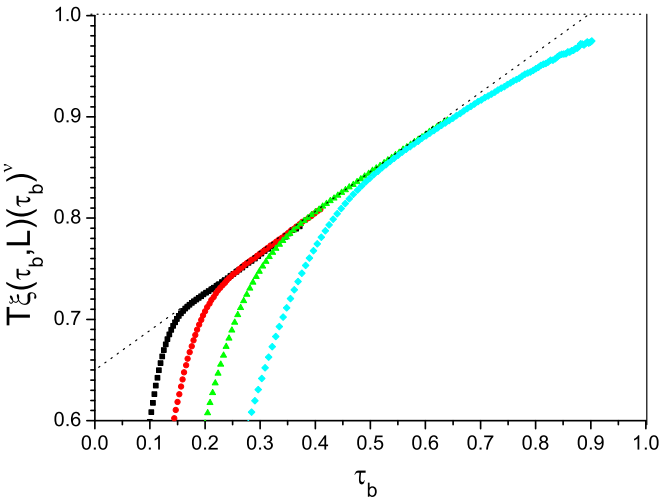

FIG. 19. The Gaussian model normalized correlation length $y = T\xi(\tau_b,L)(\tau_b)^{\nu_b}$ with $\nu_b = 1.28$ against $x = \tau_b$, see text. Sizes $L = 128$ black squares, $L = 64$ red circles, $L = 32$ green triangles, $L16$ cyan diamonds, curves left to right. Diagonal dashed line $y(x) = 0.65(1 + 0.61x)$. The exact infinite temperature limit is $x = 1, y = 1$.

model observable $\partial \ln[T\xi(\tau_b,L)]/\partial \ln \tau_b$, Fig. 7, where the estimated value of the critical exponent from the present data is very close to $\nu_b = 1.28$, consistent with $\nu_b = (\nu - 1)/2$, with $\nu = 3.55$ the mean literature value [8]. With a single Wegner correction term the appropriate thermodynamic limit expression for the correlation length with τ_b scaling is

$$T\xi(\tau_b) = K(\tau_b)^{-\nu_b}\left(1 + a\tau_b^{\theta}\right), \tag{B3}$$

where K and a are constants and θ is the correction exponent. The equation can be rewritten as

$$[T\xi(\tau_b)](\tau_b)^{\nu_b} = K\left(1 + a\tau_b^{\theta}\right). \tag{B4}$$

Taking the derivative of Eq. (B3),

$$\frac{\partial \ln[T\xi(\tau_b,L)]}{\partial \ln(\tau_b)} = \nu_b - \frac{a\theta\tau_b^{\theta}}{\left(1 + a\tau_b^{\theta}\right)} \tag{B5}$$

$$\approx \nu_b - a\theta\tau_b^{\theta} + a^2\theta\tau_b^{2\theta}, \tag{B6}$$

where the first expression is exact. First, from a plot of the data in the form $y = [T\xi(\tau_b)](\tau_b)^{\nu_b}$ against $x = \tau_b$, a direct estimate for the correction exponent θ can be obtained because $y(x) = K + Kax^{\theta}$.

Suppose that we accept $\nu_b = 1.28$ is correct. It turns out that the data for this $y(x)$ in the Gaussian model show that a linear leading correction term dominates over a wide range of temperature (see Fig. 19). This implies the leading and subleading correction terms in $\partial \ln[T\xi(\tau_b,L)]/\partial \ln \tau_b$, Fig. 7, have exponents 1 and 2 [see (B6)], which justifies *a posteriori* the polynomial extrapolation for this particular observable (for which higher-order corrections happen to be exceptionally weak). As the leading correction exponent in a given model is the same for all observables [39], having a leading term linear in τ_b in the extrapolation polynomials for the other observables is also justified. Unfortunately, effective subleading Wegner corrections can have exponents which vary from observable to observable; we can note that attempting to estimate subleading correction exponents in ISGs in any dimension is a very hazardous task. The assumption of an exponent 2 for the next term in the polynomial in the general 2D case is a convenient approximation, justified empirically by the excellent agreement between the Gaussian intercepts estimated from the polynomial fits and the values expected knowing $\nu \approx 3.55$ [8]. We see no way to improve on the extrapolation procedure until data on still larger sizes become available.

[1] A. K. Hartmann and A. P. Young, Phys. Rev. B **64**, 180404(R) (2001).
[2] M. Ohzeki and H. Nishimori, J. Phys. A: Math. Theor. **42**, 332001 (2009).
[3] T. Jörg, J. Lukic, E. Marinari, and O. C. Martin, Phys. Rev. Lett. **96**, 237205 (2006).
[4] J. Lukic, A. Galluccio, E. Marinari, O. C. Martin, and G. Rinaldi, Phys. Rev. Lett. **92**, 117202 (2004).
[5] C. K. Thomas, D. A. Huse, and A. A. Middleton, Phys. Rev. Lett. **107**, 047203 (2011).
[6] I. A. Campbell, K. Hukushima, and H. Takayama, Phys. Rev. Lett. **97**, 117202 (2006).
[7] H. Rieger, L. Santen, U. Blasum, M. Diehl, M. Jünger, and G. Rinaldi, J. Phys. A **29**, 3939 (1996); **30**, 8795(E) (1997).
[8] A. K. Hartmann and A. P. Young, Phys. Rev. B **66**, 094419 (2002).
[9] A. C. Carter, A. J. Bray, and M. A. Moore, Phys. Rev. Lett. **88**, 077201 (2002).
[10] C. Amoruso, E. Marinari, O. C. Martin, and A. Pagnani, Phys. Rev. Lett. **91**, 087201 (2003).

[11] J. Houdayer and A. K. Hartmann, Phys. Rev. B **70**, 014418 (2004).
[12] A. K. Hartmann, A. J. Bray, A. C. Carter, M. A. Moore, and A. P. Young, Phys. Rev. B **66**, 224401 (2002).
[13] J. Poulter and J. A. Blackman, Phys. Rev. B **72**, 104422 (2005).
[14] C. K. Thomas and A. A. Middleton, Phys. Rev. B **76**, 220406(R) (2007).
[15] H. G. Katzgraber, Lik Wee Lee, and I. A. Campbell, Phys. Rev. B **75**, 014412 (2007).
[16] R. Fisch, J. Stat. Phys. **128**, 1113 (2007).
[17] A. K. Hartmann, Phys. Rev. B **77**, 144418 (2008).
[18] W. L. McMillan, Phys. Rev. B **28**, 5216 (1983).
[19] J. Houdayer, Eur. Phys. J. B **22**, 479 (2001).
[20] H. G. Katzgraber and Lik Wee Lee, Phys. Rev. B **71**, 134404 (2005).
[21] K. Hukushima and K. Nemoto, J. Phys. Soc. Jpn. **65**, 1604 (1996).
[22] I. A. Campbell, A. K. Hartmann, and H. G. Katzgraber, Phys. Rev. B **70**, 054429 (2004).
[23] J.-S. Wang, Phys. Rev. E **72**, 036706 (2005).
[24] J.-S. Wang and R. H. Swendsen, Phys. Rev. B **38**, 4840 (1988).
[25] L. Saul and M. Kardar, Phys. Rev. E **48**, R3221 (1993).
[26] W. Atisattapong and J. Poulter, New J. Phys. **10**, 093012 (2008).
[27] R. J. Baxter, *Exactly Solved Models in Statistical Mechanics* (Academic Press, London, 1982).
[28] H. G. Katzgraber, I. A. Campbell, and A. K. Hartmann, Phys. Rev. B **78**, 184409 (2008).
[29] I. A. Campbell and P. H. Lundow, Phys. Rev. B **83**, 014411 (2011).
[30] S. Caracciolo, R. G. Edwards, S. J. Ferreira, A. Pelissetto, and A. D. Sokal, Phys. Rev. Lett. **74**, 2969 (1995).
[31] F. Parisen Toldin, A. Pelissetto, and E. Vicari, Phys. Rev. E **82**, 021106 (2010).
[32] F. Parisen Toldin, A. Pelissetto, and E. Vicari, Phys. Rev. E **84**, 051116 (2011).
[33] P. H. Lundow and I. A. Campbell, Phys. Rev. E **91**, 042121 (2015); Physica A **434**, 181 (2015).
[34] T. Jörg and F. Krzakala, J. Stat. Mech. (2012) L01001.
[35] R. R. P. Singh and S. Chakravarty, Phys. Rev. B **36**, 559 (1987).
[36] L. Klein, J. Adler, A. Aharony, A. B. Harris, and Y. Meir, Phys. Rev. B **43**, 11249 (1991).
[37] D. Daboul, I. Chang, and A. Aharony, Eur. Phys. J. B **41**, 231 (2004).
[38] J. G. Darboux, J. Math. Pure Appl. **4**, 377 (1878).
[39] F. J. Wegner, Phys. Rev. B **5**, 4529 (1972).
[40] P. Butera and M. Comi, Phys. Rev. B **65**, 144431 (2002).
[41] I. A. Campbell, K. Hukushima, and H. Takayama, Phys. Rev. B **76**, 134421 (2007).
[42] I. A. Campbell and P. Butera, Phys. Rev. B **78**, 024435 (2008).
[43] P. H. Lundow and I. A. Campbell, Phys. Rev. B **83**, 184408 (2011).
[44] B. Berche, C. Chatelain, C. Dhall, R. Kenna, R. Low, and J. C. Walter, J. Stat. Mech. (2008) P11010.
[45] V. Privman, P. C. Hohenberg, and A. Aharony, Universal Critical-Point Amplitude Relations, in *Phase Transitions and Critical Phenomena*, edited by C. Domb and J. L. Lebowitz (Academic Press, New York, 1991), Vol. 14, p. 1.